Measurement of the ZZ production cross section using the full CDF II data set

T. Aaltonen,[21] S. Amerio[jj],[39] D. Amidei,[31] A. Anastassov[v],[15] A. Annovi,[17] J. Antos,[12] G. Apollinari,[15] J.A. Appel,[15] T. Arisawa,[52] A. Artikov,[13] J. Asaadi,[47] W. Ashmanskas,[15] B. Auerbach,[2] A. Aurisano,[47] F. Azfar,[38] W. Badgett,[15] T. Bae,[25] A. Barbaro-Galtieri,[26] V.E. Barnes,[43] B.A. Barnett,[23] P. Barria[ll],[41] P. Bartos,[12] M. Bauce[jj],[39] F. Bedeschi,[41] S. Behari,[15] G. Bellettini[kk],[41] J. Bellinger,[54] D. Benjamin,[14] A. Beretvas,[15] A. Bhatti,[45] K.R. Bland,[5] B. Blumenfeld,[23] A. Bocci,[14] A. Bodek,[44] D. Bortoletto,[43] J. Boudreau,[42] A. Boveia,[11] L. Brigliadori[ii],[6] C. Bromberg,[32] E. Brucken,[21] J. Budagov,[13] H.S. Budd,[44] K. Burkett,[15] G. Busetto[jj],[39] P. Bussey,[19] P. Butti[kk],[41] A. Buzatu,[19] A. Calamba,[10] S. Camarda,[4] M. Campanelli,[28] F. Canelli[cc],[11] B. Carls,[22] D. Carlsmith,[54] R. Carosi,[41] S. Carrillo[l],[16] B. Casal[j],[9] M. Casarsa,[48] A. Castro[ii],[6] P. Catastini,[20] D. Cauz[qqrr],[48] V. Cavaliere,[22] M. Cavalli-Sforza,[4] A. Cerri[e],[26] L. Cerrito[q],[28] Y.C. Chen,[1] M. Chertok,[7] G. Chiarelli,[41] G. Chlachidze,[15] K. Cho,[25] D. Chokheli,[13] A. Clark,[18] C. Clarke,[53] M.E. Convery,[15] J. Conway,[7] M. Corbo[y],[15] M. Cordelli,[17] C.A. Cox,[7] D.J. Cox,[7] M. Cremonesi,[41] D. Cruz,[47] J. Cuevas[x],[9] R. Culbertson,[15] N. d'Ascenzo[u],[15] M. Datta[ff],[15] P. de Barbaro,[44] L. Demortier,[45] M. Deninno,[6] M. D'Errico[jj],[39] F. Devoto,[21] A. Di Canto[kk],[41] B. Di Ruzza[p],[15] J.R. Dittmann,[5] S. Donati[kk],[41] M. D'Onofrio,[27] M. Dorigo[ss],[48] A. Driutti[qqrr],[48] K. Ebina,[52] R. Edgar,[31] A. Elagin,[47] R. Erbacher,[7] S. Errede,[22] B. Esham,[22] S. Farrington,[38] J.P. Fernández Ramos,[29] R. Field,[16] G. Flanagan[s],[15] R. Forrest,[7] M. Franklin,[20] J.C. Freeman,[15] H. Frisch,[11] Y. Funakoshi,[52] C. Galloni[kk],[41] A.F. Garfinkel,[43] P. Garosi[ll],[41] H. Gerberich,[22] E. Gerchtein,[15] S. Giagu,[46] V. Giakoumopoulou,[3] K. Gibson,[42] C.M. Ginsburg,[15] N. Giokaris,[3] P. Giromini,[17] G. Giurgiu,[23] V. Glagolev,[13] D. Glenzinski,[15] M. Gold,[34] D. Goldin,[47] A. Golossanov,[15] G. Gomez,[9] G. Gomez-Ceballos,[30] M. Goncharov,[30] O. González López,[29] I. Gorelov,[34] A.T. Goshaw,[14] K. Goulianos,[45] E. Gramellini,[6] S. Grinstein,[4] C. Grosso-Pilcher,[11] R.C. Group,[51,15] J. Guimaraes da Costa,[20] S.R. Hahn,[15] J.Y. Han,[44] F. Happacher,[17] K. Hara,[49] M. Hare,[50] R.F. Harr,[53] T. Harrington-Taber[m],[15] K. Hatakeyama,[5] C. Hays,[38] J. Heinrich,[40] M. Herndon,[54] A. Hocker,[15] Z. Hong,[47] W. Hopkins[f],[15] S. Hou,[1] R.E. Hughes,[35] U. Husemann,[55] M. Hussein[aa],[32] J. Huston,[32] G. Introzzi[nnoo],[41] M. Iori[pp],[46] A. Ivanov[o],[7] E. James,[15] D. Jang,[10] B. Jayatilaka,[15] E.J. Jeon,[25] S. Jindariani,[15] M. Jones,[43] K.K. Joo,[25] S.Y. Jun,[10] T.R. Junk,[15] M. Kambeitz,[24] T. Kamon,[25,47] P.E. Karchin,[53] A. Kasmi,[5] Y. Kato[n],[37] W. Ketchum[gg],[11] J. Keung,[40] B. Kilminster[cc],[15] D.H. Kim,[25] H.S. Kim,[25] J.E. Kim,[25] M.J. Kim,[17] S.H. Kim,[49] S.B. Kim,[25] Y.J. Kim,[25] Y.K. Kim,[11] N. Kimura,[52] M. Kirby,[15] K. Knoepfel,[15] K. Kondo,[52,*] D.J. Kong,[25] J. Konigsberg,[16] A.V. Kotwal,[14] M. Kreps,[24] J. Kroll,[40] M. Kruse,[14] T. Kuhr,[24] M. Kurata,[49] A.T. Laasanen,[43] S. Lammel,[15] M. Lancaster,[28] K. Lannon[w],[35] G. Latino[ll],[41] H.S. Lee,[25] J.S. Lee,[25] S. Leo,[41] S. Leone,[41] J.D. Lewis,[15] A. Limosani[r],[14] E. Lipeles,[40] A. Lister[a],[18] H. Liu,[51] Q. Liu,[43] T. Liu,[15] S. Lockwitz,[55] A. Loginov,[55] D. Lucchesi[jj],[39] A. Lucà,[17] J. Lueck,[24] P. Lujan,[26] P. Lukens,[15] G. Lungu,[45] J. Lys,[26] R. Lysak[d],[12] R. Madrak,[15] P. Maestro[ll],[41] S. Malik,[45] G. Manca[b],[27] A. Manousakis-Katsikakis,[3] L. Marchese[hh],[6] F. Margaroli,[46] P. Marino[mm],[41] M. Martínez,[4] K. Matera,[22] M.E. Mattson,[53] A. Mazzacane,[15] P. Mazzanti,[6] R. McNulty[i],[27] A. Mehta,[27] P. Mehtala,[21] C. Mesropian,[45] T. Miao,[15] D. Mietlicki,[31] A. Mitra,[1] H. Miyake,[49] S. Moed,[15] N. Moggi,[6] C.S. Moon[y],[15] R. Moore[ddee],[15] M.J. Morello[mm],[41] A. Mukherjee,[15] Th. Muller,[24] P. Murat,[15] M. Mussini[ii],[6] J. Nachtman[m],[15] Y. Nagai,[49] J. Naganoma,[52] I. Nakano,[36] A. Napier,[50] J. Nett,[47] C. Neu,[51] T. Nigmanov,[42] L. Nodulman,[2] S.Y. Noh,[25] O. Norniella,[22] L. Oakes,[38] S.H. Oh,[14] Y.D. Oh,[25] I. Oksuzian,[51] T. Okusawa,[37] R. Orava,[21] L. Ortolan,[4] C. Pagliarone,[48] E. Palencia[e],[9] P. Palni,[34] V. Papadimitriou,[15] W. Parker,[54] G. Pauletta[qqrr],[48] M. Paulini,[10] C. Paus,[30] T.J. Phillips,[14] G. Piacentino,[41] E. Pianori,[40] J. Pilot,[7] K. Pitts,[22] C. Plager,[8] L. Pondrom,[54] S. Poprocki[f],[15] K. Potamianos,[26] A. Pranko,[26] F. Prokoshin[z],[13] F. Ptohos[g],[17] G. Punzi[kk],[41] N. Ranjan,[43] I. Redondo Fernández,[29] P. Renton,[38] M. Rescigno,[46] F. Rimondi,[6,*] L. Ristori,[41,15] A. Robson,[19] T. Rodriguez,[40] S. Rolli[h],[50] M. Ronzani[kk],[41] R. Roser,[15] J.L. Rosner,[11] F. Ruffini[ll],[41] A. Ruiz,[9] J. Russ,[10] V. Rusu,[15] W.K. Sakumoto,[44] Y. Sakurai,[52] L. Santi[qqrr],[48] K. Sato,[49] V. Saveliev[u],[15] A. Savoy-Navarro[y],[15] P. Schlabach,[15] E.E. Schmidt,[15] T. Schwarz,[31] L. Scodellaro,[9] F. Scuri,[41] S. Seidel,[34] Y. Seiya,[37] A. Semenov,[13] F. Sforza[kk],[41] S.Z. Shalhout,[7] T. Shears,[27] P.F. Shepard,[42] M. Shimojima[t],[49] M. Shochet,[11] I. Shreyber-Tecker,[33] A. Simonenko,[13] K. Sliwa,[50] J.R. Smith,[7] F.D. Snider,[15] H. Song,[42] V. Sorin,[4] R. St. Denis,[19,*] M. Stancari,[15] D. Stentz[v],[15] J. Strologas,[34] Y. Sudo,[49] A. Sukhanov,[15] I. Suslov,[13] K. Takemasa,[49] Y. Takeuchi,[49] J. Tang,[11] M. Tecchio,[31] P.K. Teng,[1] J. Thom[f],[15] E. Thomson,[40] V. Thukral,[47] D. Toback,[47] S. Tokar,[12] K. Tollefson,[32] T. Tomura,[49] D. Tonelli[e],[15] S. Torre,[17] D. Torretta,[15] P. Totaro,[39] M. Trovato[mm],[41] F. Ukegawa,[49] S. Uozumi,[25] F. Vázquez[l],[16] G. Velev,[15] C. Vellidis,[15] C. Vernieri[mm],[41] M. Vidal,[43] R. Vilar,[9] J. Vizán[bb],[9] M. Vogel,[34] G. Volpi,[17] P. Wagner,[40] R. Wallny[j],[15] S.M. Wang,[1] D. Waters,[28] W.C. Wester III,[15] D. Whiteson[c],[40] A.B. Wicklund,[2] S. Wilbur,[7] H.H. Williams,[40] J.S. Wilson,[31] P. Wilson,[15] B.L. Winer,[35] P. Wittich[f],[15] S. Wolbers,[15] H. Wolfe,[35] T. Wright,[31] X. Wu,[18] Z. Wu,[5] K. Yamamoto,[37]

arXiv:1403.2300v3 [hep-ex] 20 May 2014

D. Yamato,[37] T. Yang,[15] U.K. Yang,[25] Y.C. Yang,[25] W.-M. Yao,[26] G.P. Yeh,[15] K. Yi[m],[15] J. Yoh,[15] K. Yorita,[52] T. Yoshida[k],[37] G.B. Yu,[14] I. Yu,[25] A.M. Zanetti,[48] Y. Zeng,[14] C. Zhou,[14] and S. Zucchelli[ii6]
(CDF Collaboration)[, †]

[1]*Institute of Physics, Academia Sinica, Taipei, Taiwan 11529, Republic of China*
[2]*Argonne National Laboratory, Argonne, Illinois 60439, USA*
[3]*University of Athens, 157 71 Athens, Greece*
[4]*Institut de Fisica d'Altes Energies, ICREA, Universitat Autonoma de Barcelona, E-08193, Bellaterra (Barcelona), Spain*
[5]*Baylor University, Waco, Texas 76798, USA*
[6]*Istituto Nazionale di Fisica Nucleare Bologna, [ii] University of Bologna, I-40127 Bologna, Italy*
[7]*University of California, Davis, Davis, California 95616, USA*
[8]*University of California, Los Angeles, Los Angeles, California 90024, USA*
[9]*Instituto de Fisica de Cantabria, CSIC-University of Cantabria, 39005 Santander, Spain*
[10]*Carnegie Mellon University, Pittsburgh, Pennsylvania 15213, USA*
[11]*Enrico Fermi Institute, University of Chicago, Chicago, Illinois 60637, USA*
[12]*Comenius University, 842 48 Bratislava, Slovakia; Institute of Experimental Physics, 040 01 Kosice, Slovakia*
[13]*Joint Institute for Nuclear Research, RU-141980 Dubna, Russia*
[14]*Duke University, Durham, North Carolina 27708, USA*
[15]*Fermi National Accelerator Laboratory, Batavia, Illinois 60510, USA*
[16]*University of Florida, Gainesville, Florida 32611, USA*
[17]*Laboratori Nazionali di Frascati, Istituto Nazionale di Fisica Nucleare, I-00044 Frascati, Italy*
[18]*University of Geneva, CH-1211 Geneva 4, Switzerland*
[19]*Glasgow University, Glasgow G12 8QQ, United Kingdom*
[20]*Harvard University, Cambridge, Massachusetts 02138, USA*
[21]*Division of High Energy Physics, Department of Physics, University of Helsinki, FIN-00014, Helsinki, Finland; Helsinki Institute of Physics, FIN-00014, Helsinki, Finland*
[22]*University of Illinois, Urbana, Illinois 61801, USA*
[23]*The Johns Hopkins University, Baltimore, Maryland 21218, USA*
[24]*Institut für Experimentelle Kernphysik, Karlsruhe Institute of Technology, D-76131 Karlsruhe, Germany*
[25]*Center for High Energy Physics: Kyungpook National University, Daegu 702-701, Korea; Seoul National University, Seoul 151-742, Korea; Sungkyunkwan University, Suwon 440-746, Korea; Korea Institute of Science and Technology Information, Daejeon 305-806, Korea; Chonnam National University, Gwangju 500-757, Korea; Chonbuk National University, Jeonju 561-756, Korea; Ewha Womans University, Seoul, 120-750, Korea*
[26]*Ernest Orlando Lawrence Berkeley National Laboratory, Berkeley, California 94720, USA*
[27]*University of Liverpool, Liverpool L69 7ZE, United Kingdom*
[28]*University College London, London WC1E 6BT, United Kingdom*
[29]*Centro de Investigaciones Energeticas Medioambientales y Tecnologicas, E-28040 Madrid, Spain*
[30]*Massachusetts Institute of Technology, Cambridge, Massachusetts 02139, USA*
[31]*University of Michigan, Ann Arbor, Michigan 48109, USA*
[32]*Michigan State University, East Lansing, Michigan 48824, USA*
[33]*Institution for Theoretical and Experimental Physics, ITEP, Moscow 117259, Russia*
[34]*University of New Mexico, Albuquerque, New Mexico 87131, USA*
[35]*The Ohio State University, Columbus, Ohio 43210, USA*
[36]*Okayama University, Okayama 700-8530, Japan*
[37]*Osaka City University, Osaka 558-8585, Japan*
[38]*University of Oxford, Oxford OX1 3RH, United Kingdom*
[39]*Istituto Nazionale di Fisica Nucleare, Sezione di Padova, [jj] University of Padova, I-35131 Padova, Italy*
[40]*University of Pennsylvania, Philadelphia, Pennsylvania 19104, USA*
[41]*Istituto Nazionale di Fisica Nucleare Pisa, [kk] University of Pisa, [ll] University of Siena, [mm] Scuola Normale Superiore, I-56127 Pisa, Italy, [nn] INFN Pavia, I-27100 Pavia, Italy, [oo] University of Pavia, I-27100 Pavia, Italy*
[42]*University of Pittsburgh, Pittsburgh, Pennsylvania 15260, USA*
[43]*Purdue University, West Lafayette, Indiana 47907, USA*
[44]*University of Rochester, Rochester, New York 14627, USA*
[45]*The Rockefeller University, New York, New York 10065, USA*
[46]*Istituto Nazionale di Fisica Nucleare, Sezione di Roma 1, [pp] Sapienza Università di Roma, I-00185 Roma, Italy*
[47]*Mitchell Institute for Fundamental Physics and Astronomy, Texas A&M University, College Station, Texas 77843, USA*

[48] Istituto Nazionale di Fisica Nucleare Trieste, [qq] Gruppo Collegato di Udine,
[rr] University of Udine, I-33100 Udine, Italy, [ss] University of Trieste, I-34127 Trieste, Italy
[49] University of Tsukuba, Tsukuba, Ibaraki 305, Japan
[50] Tufts University, Medford, Massachusetts 02155, USA
[51] University of Virginia, Charlottesville, Virginia 22906, USA
[52] Waseda University, Tokyo 169, Japan
[53] Wayne State University, Detroit, Michigan 48201, USA
[54] University of Wisconsin, Madison, Wisconsin 53706, USA
[55] Yale University, New Haven, Connecticut 06520, USA

We present a measurement of the ZZ boson-pair production cross section in 1.96 TeV center-of-mass energy $p\overline{p}$ collisions. We reconstruct final states incorporating four charged leptons or two charged leptons and two neutrinos from the full data set collected by the Collider Detector experiment at the Fermilab Tevatron, corresponding to 9.7 fb^{-1} of integrated luminosity. Combining the results obtained from each final state, we measure a cross section of $1.04^{+0.32}_{-0.25}$ pb, in good agreement with the standard model prediction at next-to-leading order in the strong-interaction coupling.

I. INTRODUCTION

Measurements of production cross sections for electroweak vector boson pairs are important tests of standard model (SM) predictions in the electroweak sector. If sufficiently precise, these measurements may signal contributions from non-SM physics such as anomalous trilinear gauge couplings [1] or large extra dimensions [2], which can enhance or suppress diboson production rates.

At next-to-leading order (NLO) accuracy in the strong coupling constant α_s, the SM prediction of the ZZ production cross section for $p\overline{p}$ collisions at a center-of-mass energy of 1.96 TeV is 1.4 $\pm$ 0.1 pb [3], which is among the smallest cross sections accessible by the Tevatron experiments.

The ZZ production process was first studied at the LEP e^+e^- collider at CERN [4–7] and more recently at the Tevatron $p\overline{p}$ collider. A previous ZZ production cross section measurement from leptonic final states has been published by the CDF collaboration using 6 fb^{-1} of integrated luminosity [8], the result of which is extended here. The most recent D0 collaboration results from the four charged lepton [9] and two charged lepton plus two neutrino [10] final states, using up to 9.8 fb^{-1} and 8.6 fb^{-1} of data respectively, have been combined [9] to obtain a ZZ production cross section measurement of $1.32^{+0.32}_{-0.28}$ pb. Further studies have been performed at the LHC pp collider at CERN, where the ATLAS and CMS experiments have carried out measurements using data collected through the 2012 collider run [11–14].

In this article we present a measurement of the ZZ production cross section using the full data sample collected by the CDF II detector [15] at the Tevatron, corresponding to 9.7 fb^{-1} of integrated luminosity. Compared to previous CDF studies, we analyze the full data sample and optimize the event selection further to reduce background contributions and obtain an improved measurement accuracy. The cross section is independently measured from two leptonic final states, $\ell^+\ell^-\ell'^+\ell'^-$ and $\ell^+\ell^-\nu\overline{\nu}$, where ℓ and ℓ' indicate electrons or muons originating either from prompt decays of the Z boson or from leptonic decays of a τ lepton in cases where the Z boson decays into a τ lepton pair. The portions of the inclusive $p\overline{p} \to Z/\gamma^*Z/\gamma^*$ cross section accessible to the $\ell^+\ell^-\ell'^+\ell'^-$ and $\ell^+\ell^-\nu\overline{\nu}$ decay modes are somewhat different due to the absence of γ^* couplings to neutrinos. In order to combine the measurements, both are extrapolated to an inclusive ZZ production cross section assuming the zero-width approximation, where the contributions from $\gamma^*\gamma^*$ production and $Z\gamma^*$ interference are set to zero. Henceforth, we use ZZ to denote the inclusive $Z/\gamma^*Z/\gamma^*$ production process.

*Deceased
†With visitors from [a] University of British Columbia, Vancouver, BC V6T 1Z1, Canada, [b] Istituto Nazionale di Fisica Nucleare, Sezione di Cagliari, 09042 Monserrato (Cagliari), Italy, [c] University of California Irvine, Irvine, CA 92697, USA, [d] Institute of Physics, Academy of Sciences of the Czech Republic, 182 21, Czech Republic, [e] CERN, CH-1211 Geneva, Switzerland, [f] Cornell University, Ithaca, NY 14853, USA, [g] University of Cyprus, Nicosia CY-1678, Cyprus, [h] Office of Science, U.S. Department of Energy, Washington, DC 20585, USA, [i] University College Dublin, Dublin 4, Ireland, [j] ETH, 8092 Zürich, Switzerland, [k] University of Fukui, Fukui City, Fukui Prefecture, Japan 910-0017, [l] Universidad Iberoamericana, Lomas de Santa Fe, México, C.P. 01219, Distrito Federal, [m] University of Iowa, Iowa City, IA 52242, USA, [n] Kinki University, Higashi-Osaka City, Japan 577-8502, [o] Kansas State University, Manhattan, KS 66506, USA, [p] Brookhaven National Laboratory, Upton, NY 11973, USA, [q] Queen Mary, University of London, London, E1 4NS, United Kingdom, [r] University of Melbourne, Victoria 3010, Australia, [s] Muons, Inc., Batavia, IL 60510, USA, [t] Nagasaki Institute of Applied Science, Nagasaki 851-0193, Japan, [u] National Research Nuclear University, Moscow 115409, Russia, [v] Northwestern University, Evanston, IL 60208, USA, [w] University of Notre Dame, Notre Dame, IN 46556, USA, [x] Universidad de Oviedo, E-33007 Oviedo, Spain, [y] CNRS-IN2P3, Paris, F-75205 France, [z] Universidad Tecnica Federico Santa Maria, 110v Valparaiso, Chile, [aa] The University of Jordan, Amman 11942, Jordan, [bb] Universite catholique de Louvain, 1348 Louvain-La-Neuve, Belgium, [cc] University of Zürich, 8006 Zürich, Switzerland, [dd] Massachusetts General Hospital, Boston, MA 02114 USA, [ee] Harvard Medical School, Boston, MA 02114 USA, [ff] Hampton University, Hampton, VA 23668, USA, [gg] Los Alamos National Laboratory, Los Alamos, NM 87544, USA, [hh] Università degli Studi di Napoli Federico I, I-80138 Napoli, Italy

The article is structured as follows. Section II contains a brief description of the CDF II detector. Section III discusses how ZZ events are identified in the detector. Sections IV and V describe the measurement techniques used for the $\ell^+\ell^-\ell^{(\prime)+}\ell^{(\prime)-}$ and $\ell^+\ell^-\nu\overline{\nu}$ final states, respectively. The combination of the two measurements used to obtain the final production cross section result is described in Section VI.

II. THE CDF II DETECTOR

The components of the CDF II detector relevant to this analysis are briefly described below, while a complete description can be found elsewhere [15]. The detector geometry is described using the azimuthal angle ϕ and the pseudorapidity $\eta \equiv -\ln(\tan\theta/2)$, where θ is the polar angle of a particle's trajectory with respect to the proton beam axis (positive z-axis). The pseudorapidity relative to the center of the detector is referred to as $\eta_{\rm det}$. Transverse energy and momentum are defined as $E_T \equiv E\sin\theta$ and $p_T \equiv p\sin\theta$, where E is the energy measured in a calorimeter tower (or related to an energy cluster) and p is a charged particle momentum. The trajectories of charged particles (tracks) are reconstructed using silicon micro-strip detectors [16] and a 96-layer open-cell drift chamber (COT) [17] located in a 1.4 T solenoidal magnetic field. The plateau of the drift chamber acceptance covers $|\eta_{\rm det}| \leq 1$. The inner silicon tracker provides coverage of up to 8 layers with radii between 1.35 cm and 28 cm in the region $|\eta_{\rm det}| \leq 2$. Electromagnetic (EM) and hadronic (HAD) sampling calorimeters segmented in a projective-tower geometry are located outside the solenoid. At depths corresponding to one hadronic-interaction length (λ), which is equivalent to 18–20 radiation lengths (X_0), lead absorber is used to measure the electromagnetic component of showers, while in the region 4.5–7 λ iron is used to contain the hadronic component. A central calorimeter covers the pseudorapidity region $|\eta_{\rm det}| \leq 1.1$, and a forward calorimeter extends the coverage into the region $1.1 \leq |\eta_{\rm det}| \leq 3.6$. Shower-maximum detectors (SMX) embedded in the electromagnetic calorimeters at a depth approximately corresponding to 6 X_0 assist in the position measurement and background suppression for electrons. Drift chambers and scintillators are located outside the calorimeter to identify muons, which approximate minimum-ionizing particles and typically deposit only a fraction of their energy in the absorber material.

III. EVENT RECONSTRUCTION

We collect ZZ candidate events using an online event-selection system (trigger) that records events satisfying at least one of several high-p_T lepton requirements. The central electron trigger requires an EM energy deposit (clustered among towers in the calorimeter) with $E_T \geq 18$ GeV matched to a charged particle with $p_T \geq 8$ GeV/c. Several muon triggers based on muon drift-chamber track segments (*stubs*) matched to charged particles with $p_T \geq 18$ GeV/c are also incorporated. Trigger selection efficiencies are measured from collected event samples containing leptonic W and Z boson decays [18].

We use three complementary track pattern recognition algorithms distinguished by their starting point: hits in the COT, hits in the silicon tracker, or the projections of observed calorimeter energy clusters back to the interaction region (calorimeter-seeded tracks). Electrons are identified by matching a reconstructed track to an energy cluster reconstructed in the EM calorimeters. Muons are identified by matching a track to an energy deposit in the calorimeter consistent with originating from a minimum-ionizing particle, with or without an associated stub in the muon system. All leptons are required to be isolated such that the sum of additional E_T from calorimeter towers in a cone of $\Delta R = \sqrt{\Delta\eta^2 + \Delta\phi^2} \leq 0.4$ around the lepton is less than 10% of the electron E_T or muon p_T. In order to preserve pairs of leptons in close proximity to one another, if an additional muon or electron candidate is found within the $\Delta R \leq 0.4$ cone, calorimeter towers associated with it are not included in the E_T sum. An explicit requirement that the ΔR among all the reconstructed leptons is greater than 0.05 guarantees that any two different leptons are not based on the same track.

Electron candidates are required to have a ratio of HAD-to-EM energy consistent with an electromagnetic shower and are referred to as either *central* or *forward*, depending on whether they are identified within the central or forward calorimeter. Central electron identification requires a high-quality charged particle in the COT with $p_T \geq 10$ GeV/c, projecting to the geometrical acceptance of the central SMX detector, and matched to an EM energy cluster in the central calorimeter. Central electron candidates are selected using a likelihood method to combine electron identification variables into a single discriminant. A forward electron candidate is required to be detected within the geometrical acceptance of the forward SMX detector and to be associated with energy deposits consistent with those expected for an electron in both the forward calorimeter towers and SMX detector. In order to reduce background from photons matched to misreconstructed calorimeter-seeded tracks, for each forward electron candidate we also require that the matching calorimeter-seeded track is consistent with a track formed only from hits in the silicon detector. A forward electron candidate that fails one or more of these requirements can still be selected using a likelihood-based method similar to that used for central electron selection.

Forward ($\eta_{\rm det} \geq 1.2$) muon reconstruction incorporates strict requirements on the number of COT hits and the χ^2 of the track fit to suppress background from in-flight decays of pions and kaons. The track's point of closest approach is also required to be consistent with the

$p\overline{p}$ interaction point to suppress background from cosmic rays.

We also identify charged lepton candidates from reconstructed tracks, which neither geometrically extrapolate to the instrumented region of the calorimeter nor match to track stubs in the muon detectors. Such track-based candidates are required to satisfy the same quality requirements applied to the stubless muon candidates in the region $|\eta_{\rm det}| \leq 1.2$. Due to the lack of calorimeter information, electrons and muons cannot be reliably differentiated in this region, and these lepton candidates are therefore treated as being of either lepton flavor in the Z candidate selection. Electron or track-lepton candidates are rejected if they are consistent with having originated from a photon conversion, as indicated by the presence of an additional nearby track.

The efficiencies for the aforementioned lepton selection criteria are evaluated in data and Monte Carlo simulation using inclusive $Z \to \ell\ell$ event samples. The ratio of the efficiencies determined from the simulated and collision data samples is applied as a correction factor to the modeled rates of the contributing background and ZZ signal processes.

To identify the presence of neutrinos we define the missing transverse energy as $\not\!\!E_T = |\sum_i E_{T,i}\hat{n}_{T,i}|$, where $\hat{n}_{T,i}$ is the transverse component of the unit vector pointing from the interaction point to calorimeter tower i. The $\not\!\!E_T$ is corrected for the momentum of muons, which do not deposit all of their energy in the calorimeters, and for tracks that extrapolate to uninstrumented regions of the calorimeters.

Collimated clusters of particles (*jets*) are reconstructed from energy deposits in the calorimeters using the JETCLU cone algorithm [19] with a clustering radius of $\Delta R \equiv \sqrt{\Delta\eta^2 + \Delta\phi^2} = 0.4$. Their measured energies are corrected to match, on average, that of the showering parton using standard techniques [20]. Jets are selected if they have $E_T \geq 15$ GeV and $|\eta| \leq 2.4$.

IV. $ZZ \to \ell^+\ell^-\ell^{(\prime)+}\ell^{(\prime)-}$ ANALYSIS

A. Event selection

The $ZZ \to \ell^+\ell^-\ell^{(\prime)+}\ell^{(\prime)-}$ candidate events are required to have exactly four reconstructed leptons with $p_T \geq 10$ GeV/c, at least one of which must have $p_T \geq 20$ GeV/c and satisfy the trigger requirements. The leptons are grouped into opposite-charge and same-flavor pairs, treating the track-only lepton candidates as either electrons or muons, with the objective of identifying the leptonic decay products from each Z boson decay. If an event has more than one possible pairing combination, the one for which the invariant masses of the two dilepton pairs lie closest to the known Z boson mass [21], M_Z, is chosen by minimizing $f(M_{1,2}, M_{3,4}) = (M_{1,2} - M_Z)^2 + (M_{3,4} - M_Z)^2$, where $M_{1,2}$, $M_{3,4}$ are the two reconstructed dilepton masses. One pair of leptons is required to have a reconstructed invariant mass within 15 GeV/c^2 of the known Z boson mass, while the other is required to be within 50 GeV/c^2. The $ZZ \to \ell^+\ell^-\ell^{(\prime)+}\ell^{(\prime)-}$ acceptance is determined from a PYTHIA-based Monte Carlo simulation [22] followed by a GEANT-based simulation of the CDF II detector [23]. The CTEQ5L parton distribution functions (PDFs) are used to model the momentum distribution of the initial-state partons [24].

B. Background estimation

The only significant background contribution to the $\ell^+\ell^-\ell^{(\prime)+}\ell^{(\prime)-}$ final state is Drell-Yan (DY) production of a single Z/γ^* boson in association with additional parton jets or photons that are misidentified as two additional leptons in the detector (*fakes*). A data control sample is relied upon for estimating this contribution, since the simulation is not expected to accurately model the detector effects leading to the misidentification of showering partons as leptons. In event samples collected with jet-based triggers, we measure the probability for a jet to be identified as a lepton, correcting for the contribution of prompt leptons originating from W and Z boson decays. The misidentification rate is measured as a function of lepton transverse energy, pseudorapidity, and flavor [25]. Data events with three identified leptons and a lepton-like jet [26], 3ℓ+j_ℓ, and two identified leptons and two lepton-like jets, 2ℓ+$2j_\ell$ that satisfy all other selection criteria are weighted by the measured misidentification rates associated with each lepton-like jet to provide an estimate of the background contribution. A $\mathcal{O}(1\%)$ correction is applied to account for double-counting due to the fraction of observed 3ℓ+j_ℓ events that originate from 2ℓ+$2j_\ell$ events where a single lepton-like jet is identified as a lepton.

Table I summarizes expected and observed event yields for the full data sample, corresponding to 9.7 fb^{-1} of integrated luminosity. Comparisons of the predicted and observed distributions of the most relevant kinematic variables in events passing the full $\ell^+\ell^-\ell^{(\prime)+}\ell^{(\prime)-}$ selection criteria are shown in Fig. 1. The agreement between the predicted and observed distributions indicates that the observed events are compatible with having originated from ZZ production.

C. Systematic uncertainties

We account for sources of systematic uncertainty on the simulated detector acceptance of the signal and modeling of the background processes. We assign a 2.5% uncertainty on the ZZ signal acceptance from higher-order amplitudes not included in the simulation, comparing the acceptance of a NLO calculation with the leading order (LO) simulation used for this analysis. In addition, a

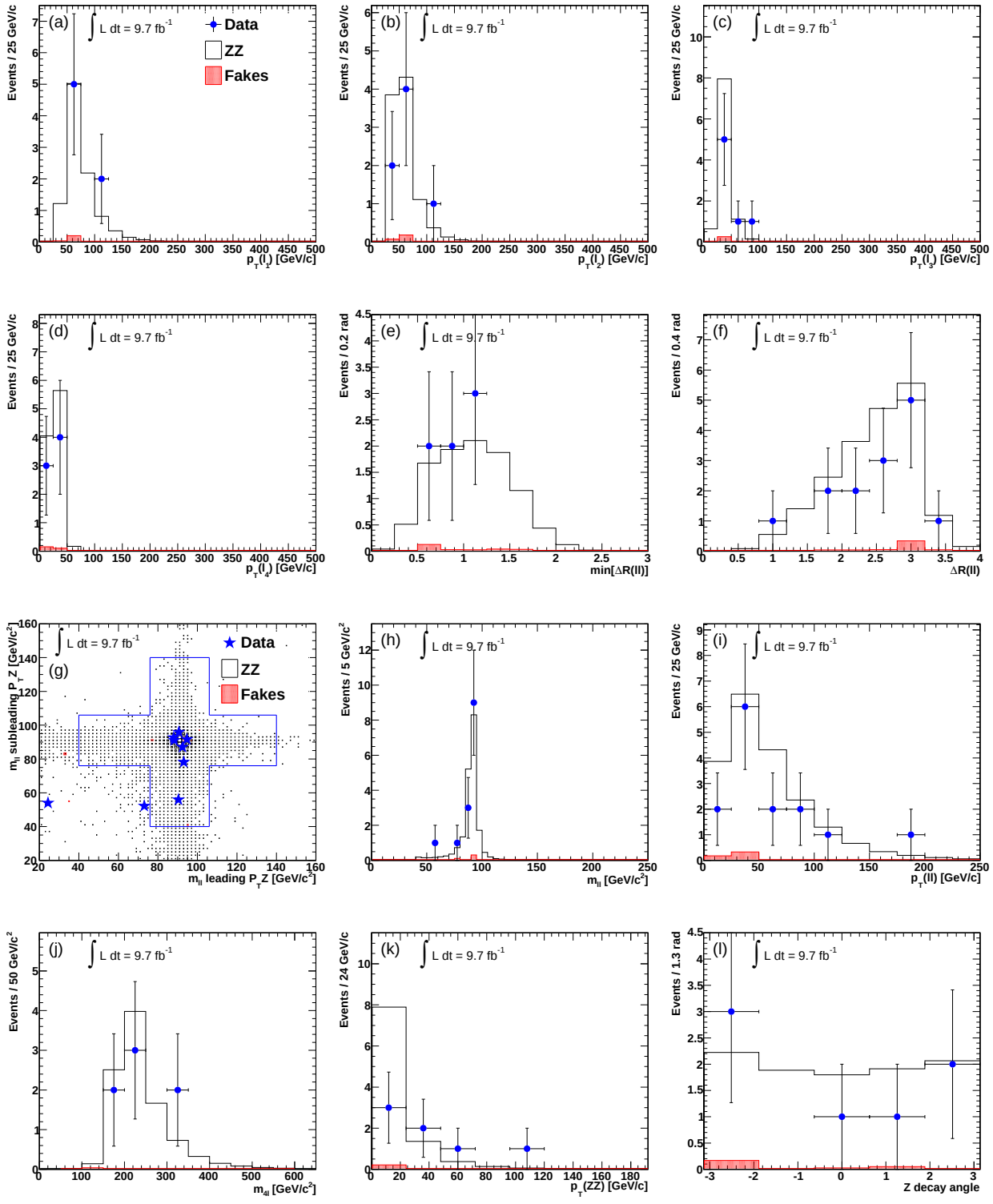

FIG. 1: Comparisons of predicted and observed distributions of kinematic variables in events passing the full $\ell^+\ell^-\ell^{(\prime)+}\ell^{(\prime)-}$ selection criteria: (a) transverse momentum of the leading lepton, (b) transverse momentum of the subleading lepton, (c) transverse momentum of the subsubleading lepton, (d) transverse momentum of the subsubsubleading lepton, (e) minimum ΔR between all possible lepton pairings, (f) opening angle ΔR between the two Z boson candidates, (g) scatter distribution of the two reconstructed dilepton invariant masses, (h) invariant masses of lepton pairs associated with both Z boson candidates, (i) transverse momenta of both Z boson candidates, (j) four lepton invariant mass, (k) transverse momentum of the ZZ system, and (l) opening angle between the two Z boson candidate decay product planes.

TABLE I: Predicted and observed numbers of $ZZ \to \ell^+\ell^-\ell^{(\prime)+}\ell^{(\prime)-}$ candidate events for the full CDF II data sample. The uncertainties on the predictions include both statistical and systematic contributions added in quadrature.

Process	Yield
ZZ	9.59 ± 1.55
DY	0.06 ± 0.03
Total expected	9.65 ± 1.55
Data	7

2.7% uncertainty is assigned to cover variations among different PDF model inputs on the simulation. We also assign a 5.9% uncertainty to the measured integrated luminosity [27], accounting for both the uncertainties on the acceptance and operation of the luminosity monitor and the measurement of the total $p\overline{p}$ cross section at the Tevatron. The limited size of the sample used to derive lepton-identification efficiencies results in an additional 3.6% uncertainty on simulated acceptances, obtained through the propagation of this uncertainty to the efficiencies on the total acceptance. Due to the presence of four leptons in each event and the high efficiencies ($\gtrsim 90\%$) of the single lepton triggers, uncertainties on measured trigger efficiencies have a minimal ($\approx 0.04\%$) impact on the overall acceptance uncertainties. The uncertainty on the DY background contribution is evaluated by applying a range of lepton misidentification rates as measured from the control samples obtained using different trigger requirements. The resulting uncertainty on the background contribution is 50%. This has a negligible effect on the precision of the cross section measurement due to the small size of the predicted contribution.

D. Result

To extract the ZZ production cross section, a Bayesian method is employed [28], building a likelihood function that takes as inputs the expected signal acceptance, the number of expected background events, and the number of observed events passing the selection criteria described above. The resulting expression gives the Poisson probability for obtaining the observed number of events as a function of the ZZ production cross section, $\sigma(p\overline{p} \to ZZ)$, to which we assign a uniform prior probability over the range of non-negative values. The function also includes terms for truncated, Gaussian-constrained nuisance parameters corresponding to each systematic uncertainty source, which are integrated over their parameter space. The value of the cross section, relative to the SM expectation, that maximizes this probability is the result of the measurement, for which we obtain $\sigma(p\overline{p} \to ZZ)/\sigma^{\mathrm{SM-NLO}} = 0.73\ ^{+0.31}_{-0.24}$ (stat) $^{+0.08}_{-0.05}$ (syst), which corresponds to a value of $\sigma(p\overline{p} \to ZZ) = 0.99\ ^{+0.45}_{-0.35}$ (stat) $^{+0.11}_{-0.07}$ (syst) pb in the zero-width approximation.

V. $ZZ \to \ell^+\ell^-\nu\overline{\nu}$ ANALYSIS

The $ZZ \to \ell^+\ell^-\nu\overline{\nu}$ decay mode has a slightly larger branching ratio (approximately 3%). The two neutrinos produced in the decay of one Z boson cannot be directly detected, and their presence is inferred from the presence of significant $\not\!\!E_T$. The $ZZ \to \ell^+\ell^-\nu\overline{\nu}$ candidate events are required to contain exactly two oppositely-charged and same-flavor leptons. One of the two leptons has to match the requirements of a single lepton trigger and have $p_T \geq 20$ GeV/c, while the second lepton is required to have $p_T \geq 10$ GeV. The invariant mass of the dilepton pair is required to be within 15 GeV/c^2 of the known Z boson mass [21].

In Tevatron collisions the dominant source of dilepton events is inclusive DY production, which has a cross section many orders of magnitude larger than that of the signal process investigated here. The main feature that distinguishes events associated with the two processes is the presence of significant $\not\!\!E_T$ within signal events. Other background contributions come from the leptonic decays of WW and WZ boson pairs. In the $WW \to \ell\nu\ell^{(\prime)}\nu$ decay, a pair of leptons can be produced in association with a significant amount of $\not\!\!E_T$ due to the presence of the two neutrinos, while the $WZ \to \ell\nu\ell^{(\prime)+}\ell^{(\prime)-}$ decay can produce a similar signature when one of the three leptons lies outside the detector coverage and is therefore undetected. Additional, non-negligible background contributions originate from $W\gamma$ and W+jets production, where the photons or jets are misidentified as leptons, and from $t\overline{t}$ quark pair-production.

A. Event selection

In order to extract the $ZZ \to \ell^+\ell^-\nu\overline{\nu}$ signal from the background-dominated event sample, we exploit differences in the kinematic properties of signal and background events. Since $ZZ \to \ell^+\ell^-\nu\overline{\nu}$ events typically contain little additional hadronic activity, we veto events that have a jet with $E_T \geq 15$ GeV recoiling against the reconstructed Z boson candidate ($\Delta\phi(j, Z) \geq \pi/2$). Events originating from DY production typically contain $\not\!\!E_T$ generated from mismeasured energies of jets recoiling against the Z boson. By vetoing events containing these types of jets, the DY background contribution is significantly reduced with a minimal ($< 5\%$) impact on signal acceptance. This requirement also suppresses potential signal contributions from $ZZ \to \ell\ell$jj decays, whose kinematic event observables are different from those of the targeted leptonic decays. Less than a 2% fraction of events remaining after this requirement contain a jet with

$E_T \geq 15$ GeV, but the DY process is still the dominant contributor of background events to this sample.

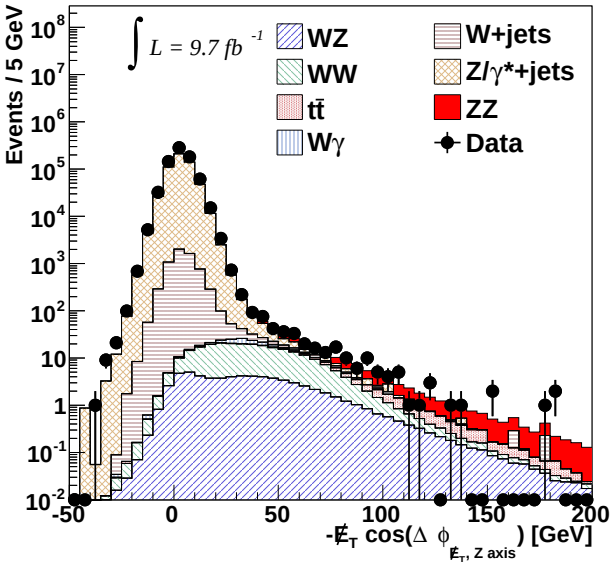

FIG. 2: Predicted and observed distributions of $\not\!\!E_T^{\rm ax}$ from selected events prior to the application of the $\not\!\!E_T^{\rm ax}$ requirement. The observed data are overlaid on stacked predictions obtained from the modeling of contributing background and signal processes.

Further separation between signal and background contributions is achieved by requiring the $\not\!\!E_T$ to be antialigned with the direction of the reconstructed Z boson p_T. We select events with $\not\!\!E_T^{\rm ax} \equiv -\not\!\!E_T \cos\Delta\phi(\hat{\not\!\!E}_T, \hat{p}_T^Z) \geq 30$ GeV, where $\Delta\phi(\hat{\not\!\!E}_T, \hat{p}_T^Z)$ is the angle between the $\vec{\not\!\!E}_T$ and the Z boson p_T. The predicted and observed distributions of $\not\!\!E_T^{\rm ax}$ in selected events are shown in Fig. 2. The predicted distributions are those obtained using the modeling described in the following section. This requirement rejects 99.8% of the remaining DY background, while preserving approximately 30% of the signal. To reduce the background contribution from processes not resulting in final-state neutrinos, in which $\not\!\!E_T$ is generated through detector mismeasurements, we also require the observed $\not\!\!E_T$ to be significant compared with the overall energy deposited in the calorimeter, $\not\!\!E_T^{\rm sig} \equiv \not\!\!E_T/\sqrt{\sum E_T} \geq 3.0$ GeV$^{1/2}$, where $\sum E_T$ represents the scalar sum of transverse energies deposited in the calorimeters. The predicted and observed distributions of $\not\!\!E_T^{\rm sig}$ in selected events are shown in Fig. 3.

B. Background estimation

Modeling of signal and background processes contributing to the $\ell^+\ell^-\nu\overline{\nu}$ final state is obtained primarily from simulation, similarly to what is done for the

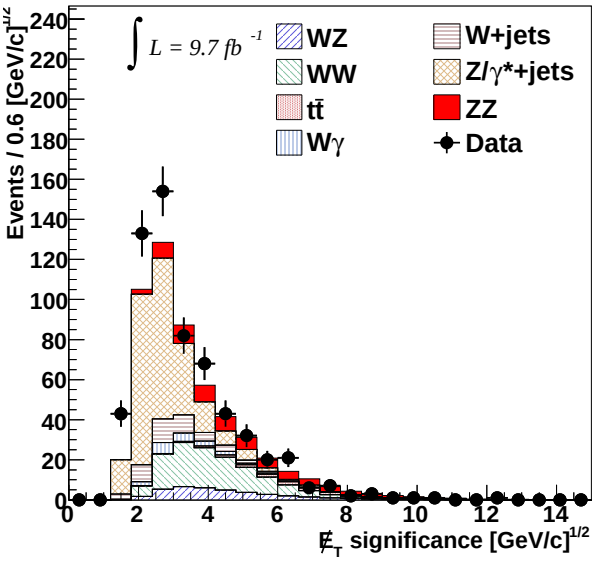

FIG. 3: Predicted and observed distributions of $\not\!\!E_T^{\rm sig}$ from selected events prior to the application of the $\not\!\!E_T^{\rm sig}$ requirement. The observed data are overlaid on stacked predictions obtained from the modeling of contributing background and signal processes.

ZZ signal in the $\ell^+\ell^-\ell^{(\prime)+}\ell^{(\prime)-}$ final state, using the CTEQ5L [24] PDF model and a GEANT-based simulation of the CDF II detector. The ZZ, WZ, DY, and $t\bar{t}$ processes are simulated using PYTHIA, while the WW process is simulated using MC@NLO [29]. The $W\gamma$ production is modeled with the Baur generator [30]. Simulated diboson and $t\bar{t}$ event samples are normalized to the highest-order theoretical cross section available [3, 31]. Normalization of the simulated DY sample is based on observed data in an independent control sample as described in more detail below. The W+jets contribution is estimated using the same data-driven method used to estimate the DY background contribution to the $\ell^+\ell^-\ell^{(\prime)+}\ell^{(\prime)-}$ final state. In this case, the same jet-to-lepton misidentification rates are applied as weights in events with one identified lepton and a lepton-like jet, 1ℓ+j_ℓ.

Table II summarizes predicted signal and background contributions to the sample after application of the selection criteria. The background contributions from DY, WW, and WZ production are reduced to levels comparable with that of the expected ZZ signal contribution.

The modeling of DY and WW background contributions is tested in independent data samples with kinematic properties similar to those of the signal sample. DY background modeling is tested using a sample of events with $\not\!\!E_T^{\rm ax} \leq 25$ GeV that otherwise satisfy the selection criteria of the signal sample with the exception of the requirement on $\not\!\!E_T^{\rm sig}$, which is not applied (low $\not\!\!E_T$ control sample). Modeling of the WW background contribution is tested using a sample of $e^\pm\mu^\mp$

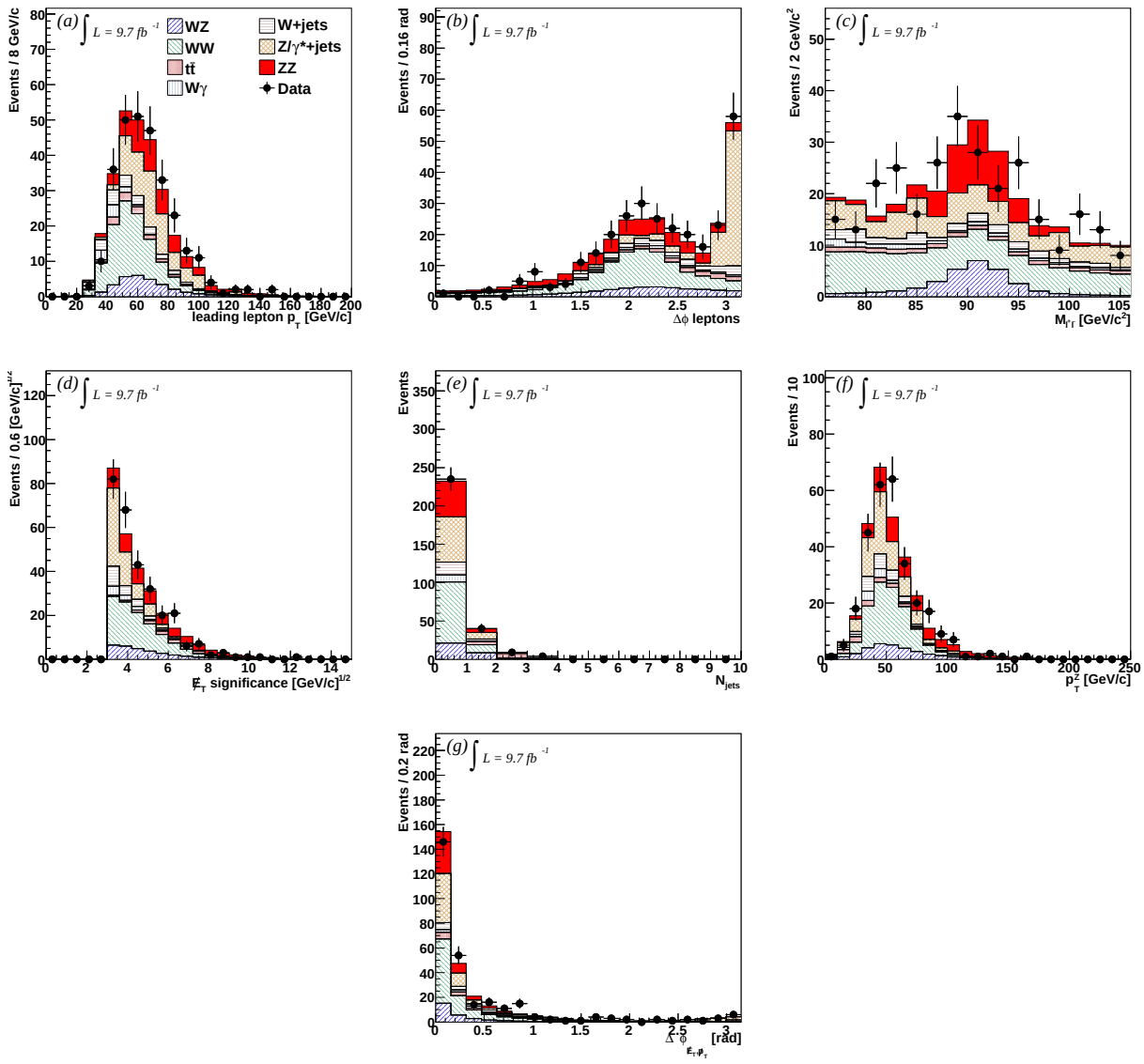

FIG. 4: Comparisons of predicted and observed distributions of kinematic variables taken as inputs to the neural network for separating signal and background contributions in events passing the full $\ell^+\ell^-\nu\overline{\nu}$ selection criteria: (a) transverse momentum of the leading lepton, (b) opening angle between the two leptons in the detector transverse plane, (c) reconstructed dilepton invariant mass, (d) $\not\!\!E_T$ significance, (e) number of reconstructed jets, (f) transverse momentum of the dilepton system, and (g) angle in the detector transverse plane between the $\not\!\!E_T$ and the $\not\!\!p_T$.

events passing the same requirements applied for signal events with the exceptions of no requirement on $\not\!\!E_T^{\rm sig}$ and restricting the dilepton invariant mass to the region $40 \leq M_{e\mu} \leq 140$ GeV/c^2 (e–μ control sample). The contribution of the ZZ signal process to each of these control samples is negligible, while the e–μ control sample contains a small, residual contribution from DY production through $Z \to \tau\tau$ decays. A normalization for the predicted DY contribution to the signal sample is obtained from the e–μ control sample by fitting the prediction to data in the high $\not\!\!E_T$ region [25]. In this kinematic region, the $\Delta\phi(\ell\ell)$ distributions of the WW and DY event contributions have different behaviors: the DY contribution, mainly coming from $Z \to \tau^+\tau^-$ decays, is peaked at $\Delta\phi(e\mu) \approx \pi$, while the contribution from WW production has a broader $\Delta\phi(e\mu)$ distribution peaked at ≈ 2. Hence, contributions from the two processes can be distinguished in this kinematic region, allowing for the extraction of a correction factor that can be applied to the predicted DY contribution in the signal sample.

C. Neural network separation

In order to further improve the separation of signal and background, we apply an artificial neural network trained

TABLE II: Predicted and observed numbers of $ZZ \to \ell^+\ell^-\nu\overline{\nu}$ candidate events for the full CDF II data sample. The uncertainties on the predictions include both statistical and systematic contributions added in quadrature.

Process	Yield
DY	67.2 ± 10.8
$t\bar{t}$	11.5 ± 2.1
W+jets	20.0 ± 5.3
$W\gamma$	9.7 ± 1.2
WW	91.2 ± 8.5
WZ	30.4 ± 4.3
Total background	230 ± 15.5
ZZ	52.5 ± 9.2
Data	288

on simulated signal and background events. The neural network takes kinematic properties of events as inputs and produces a single variable output that is indicative of the consistency of the event with either the signal or background hypotheses. We use a NeuroBayes neural network (NN) [32] trained on seven kinematic event variables, whose predicted and observed distributions for the signal sample are shown in Fig. 4. These variables are, in order of decreasing discrimination power, the leading lepton transverse momentum ($p_T(\ell_1)$), the $\not\!\!E_T$ significance ($\not\!\!E_T/\sqrt{\sum E_T}$), the dilepton invariant mass ($m_{\ell\ell}$), the dilepton system transverse momentum ($p_T^{\ell\ell}$), the opening angle between the two leptons in the transverse plane ($\Delta\phi(\ell\ell)$), the number of reconstructed jets ($N_{\rm jets}$), and the angle in the transverse plane between the $\not\!\!E_T$ based on energy deposits in the calorimeter and a similarly-defined $\not\!\!p_T$ variable based on charged tracks. A comparison of the predicted and observed distributions of the NN output variable for candidate events is shown in Fig. 5. Events consistent with having originated from the signal process are assigned NN output values near +1, while those more consistent with having originated from one of the background processes have values closer to -1.

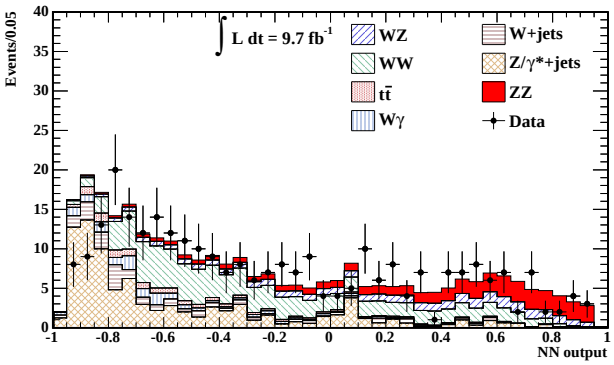

(a)

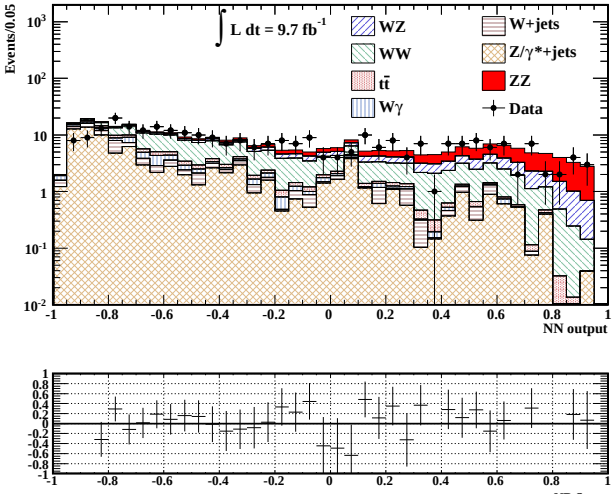

(b)

FIG. 5: Comparison of predicted and observed NN output distributions for the $\ell^+\ell^-\nu\overline{\nu}$ signal sample shown on (a) linear and (b) logarithmic scales, including a distribution of the bin-by-bin differences at the bottom.

D. Systematic uncertainties

The systematic uncertainties considered in this measurement affect both predicted signal and background contributions as well as the modeled shapes of the NN output variable distribution for each of the contributing processes. Table III summarizes the complete set of systematic uncertainties incorporated in the measurement.

The effect of missing higher-order amplitudes in the simulations used to determine detector acceptances is a significant source of uncertainty on the predicted event rates for most contributing processes. The sizes of the assigned uncertainties are obtained by comparing simulated acceptances from NLO calculations with those obtained from the LO event generators. Uncertainties associated with the PDF model taken as input to the simulation are assessed following the prescription in Ref. [33]. Uncertainties on the theoretical cross sections for WW [3], WZ [3], $W\gamma$ [34], and $t\bar{t}$ [35, 36] production, which are used to normalize the expected contributions from these processes, are also incorporated along with the 5.9% uncertainty associated with the CDF luminosity measurement [27]. Uncertainties associated with lepton identification and trigger efficiency measurements are assessed using the same methodology described previously for the measurement from the $\ell^+\ell^-\ell^{(\prime)+}\ell^{(\prime)-}$ final state. The effect of reconstructed jet energy uncertainties on acceptances, including the impact of the veto criteria on events containing reconstructed jets, is evaluated in simulation by varying the jet energy scale within its measured uncertainties.

The uncertainty assigned to the predicted W+jets background contribution is determined by varying jet

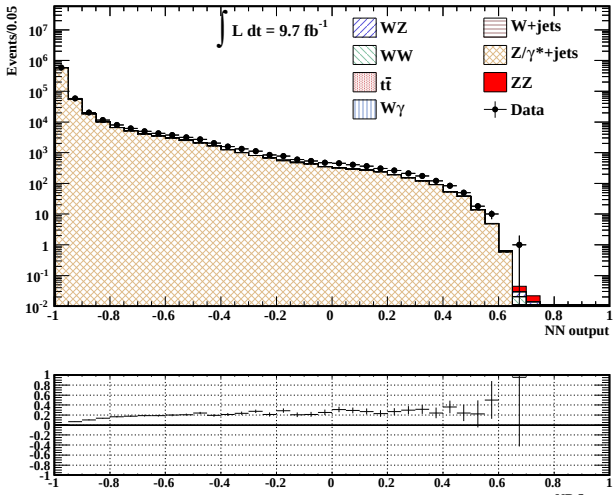

FIG. 6: Comparison of predicted and observed distributions of NN output variable for the low $\not\!\!E_T$ control sample, including a distribution of the bin-by-bin differences at the bottom.

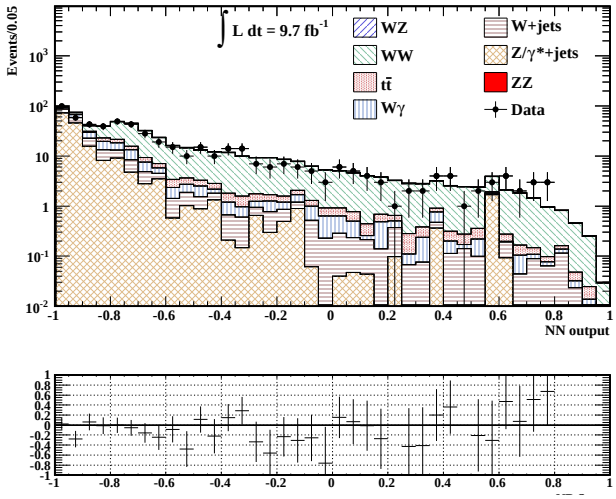

FIG. 7: Comparison of predicted and observed distributions of NN output variable for the e–μ control sample, including a distribution of the bin-by-bin differences at the bottom.

misidentification rates over the range of values obtained from samples collected with different trigger requirements. The statistical uncertainty associated with the fit performed in the high $\not\!\!E_T$ region of the e–μ control sample, used to normalize the estimated DY contribution, is taken as the systematic uncertainty on the event-yield prediction for this process.

The mismodeling of relevant kinematic distributions is accounted for by incorporating systematic uncertainties covering differences between predicted and observed shapes of the NN output variable within the previously described control regions. Figures 6 and 7 show comparisons of the predicted and observed distributions of this variable in the low $\not\!\!E_T$ and e–μ control samples. The disagreement between predicted and observed distributions in the low $\not\!\!E_T$ control sample is used to assess a shape uncertainty on the modeled NN output distribution for the DY process, which is the dominant contributor of events to this control sample. Conversely, due to the agreement between predicted and observed distributions of the NN output variable in the e–μ control sample, no shape uncertainty is assigned to the modeled NN output distribution for the WW process, from which a majority of the events in this control sample originate.

E. Result

The ZZ production cross section is extracted from a fit to the NN output variable distribution shown in Fig. 5. Following the Bayesian approach used for the measurement in the $\ell^+\ell^-\ell^{(\prime)+}\ell^{(\prime)-}$ final state, a binned likelihood function is constructed from a product of likelihoods for obtaining the results observed in each bin based on expected signal acceptance, the number of expected background events, and the number of observed events. Correlations in the signal and background expectations across bins are incorporated in the likelihood function as well as shared terms for nuisance parameters corresponding to each systematic uncertainty source. The nuisance parameters are Gaussian constrained to zero and integrated over their parameter spaces in the fit used to extract the cross section measurement. The value of the cross section that maximizes the constructed likelihood, relative to the SM cross section, is $\sigma(p\overline{p} \to ZZ)/\sigma^{\mathrm{SM-NLO}} = 0.84\ ^{+0.23}_{-0.22}\ (\mathrm{stat})\ ^{+0.16}_{-0.12}\ (\mathrm{syst})$, which corresponds to a value of $\sigma(p\overline{p} \to ZZ) = 1.18\ ^{+0.32}_{-0.31}\ (\mathrm{stat})\ ^{+0.22}_{-0.17}\ (\mathrm{syst})$ pb in the zero-width approximation.

VI. MEASUREMENT COMBINATION AND SUMMARY

We combine the independent ZZ production cross section measurements obtained from the non-overlapping $\ell^+\ell^-\ell^{(\prime)+}\ell^{(\prime)-}$ and $\ell^+\ell^-\nu\overline{\nu}$ signal samples to obtain the final result. We perform a simultaneous fit, considering the number of expected and observed events in the $\ell^+\ell^-\ell^{(\prime)+}\ell^{(\prime)-}$ sample and the predicted and observed binned NN output variable distributions from events in the $\ell^+\ell^-\nu\overline{\nu}$ sample. The combination procedure takes into account correlations from common systematic uncertainty sources affecting signal and background expectations in the two samples. The combined result is

$$\sigma(p\overline{p} \to ZZ) = 1.04^{+0.32}_{-0.25}\ (\mathrm{stat} + \mathrm{syst})\ \mathrm{pb}\ ,$$

which is consistent with the SM expectation of $\sigma^{\mathrm{NLO}}_{ZZ} = 1.4 \pm 0.1$ pb. This result, based on the full

TABLE III: Systematic uncertainties incorporated in the cross section measurement using the $\ell^+\ell^-\nu\overline{\nu}$ signal sample. All uncertainties are expressed in percents, other than the check mark, representing the shape uncertainty considered on the DY simulated prediction.

Source	ZZ	WW	WZ	$t\bar{t}$	DY	$W\gamma$	W+jets
Theoretical cross section		6	6	10		10	
Run-dependence modeling				10			
PDF modeling	2.7	1.9	2.7	2.1		2.2	
Higher-order amplitudes	5		5	10		5	
Luminosity	5.9	5.9	5.9	5.9		5.9	
Photon conversion modeling						10	
Jet energy scale	2.0	1.6	3.4	5.3		2.0	
Jet to lepton misidentification rate							16
Lepton identification efficiency	3	3	3	3			
Trigger efficiency	2	2	2	2			
DY normalization					10.2		
DY mismodeling					✓		

CDF II data set, approaches the limit in precision achievable at the Tevatron, being primarily limited by the size of the available data set.

VII. ACKNOWLEDGMENTS

We thank the Fermilab staff and the technical staffs of the participating institutions for their vital contributions. This work was supported by the U.S. Department of Energy and National Science Foundation; the Italian Istituto Nazionale di Fisica Nucleare; the Ministry of Education, Culture, Sports, Science and Technology of Japan; the Natural Sciences and Engineering Research Council of Canada; the National Science Council of the Republic of China; the Swiss National Science Foundation; the A.P. Sloan Foundation; the Bundesministerium für Bildung und Forschung, Germany; the Korean World Class University Program, the National Research Foundation of Korea; the Science and Technology Facilities Council and the Royal Society, United Kingdom; the Russian Foundation for Basic Research; the Ministerio de Ciencia e Innovación, and Programa Consolider-Ingenio 2010, Spain; the Slovak R&D Agency; the Academy of Finland; the Australian Research Council (ARC); and the EU community Marie Curie Fellowship Contract No. 302103.

[1] K. Hagiwara, R. D. Peccei, D. Zeppenfeld, and K. Hikasa, Nuclear Physics **B282**, 253 (1987).
[2] M. Kober, B. Koch, and M. Bleicher, Phys. Rev. D **76**, 125001 (2007).
[3] J. Campbell and R. K. Ellis, Phys. Rev. D **60**, 113006 (1999). We use the MCFM Monte Carlo with the MSTW2008 PDF set and varying the factorization and renormalization scales.
[4] R. Barate *et al.* (ALEPH Collaboration), Phys. Lett. B **469**, 287 (1999).
[5] J. Abdallah *et al.* (DELPHI Collaboration), Eur. Phys. J. C **30**, 447 (2003).
[6] M. Acciarri *et al.* (L3 Collaboration), Phys. Lett. B **465**, 363 (1999).
[7] G. Abbiendi *et al.* (OPAL Collaboration), Eur. Phys. J. C **32**, 303 (2003).
[8] T. Aaltonen *et al.* (CDF Collaboration), Phys. Rev. Lett. **108**, 101801 (2012).
[9] V. M. Abazov *et al.* (D0 Collaboration), Phys. Rev. D **88**, 032008 (2013).
[10] V. Abazov *et al.* (D0 Collaboration), Phys. Rev. D **85**, 112005 (2012).
[11] G. Aad *et al.* (ATLAS Collaboration), Phys. Rev. Lett. **108**, 041804 (2012).
[12] G. Aad *et al.* (ATLAS Collaboration), J. High Energy Phys. 03 (2013) 128.
[13] S. Chatrchyan *et al.* (CMS Collaboration), Phys. Lett. B **721**, 190 (2013).
[14] S. Chatrchyan *et al.* (CMS Collaboration), J. High Energy Phys. 01 (2013) 063.
[15] D. Acosta *et al.* (CDF Collaboration), Phys. Rev. D **71**, 032001 (2005).
[16] T. Aaltonen *et al.*, Nucl. Instrum. Methods A **729**, 153 (2013).
[17] T. Affolder *et al.*, Nucl. Instrum. Methods A **526**, 249 (2004).
[18] D. Acosta *et al.* (CDF Collaboration), Phys. Rev. Lett. **94**, 091803 (2005).
[19] F. Abe *et al.* (CDF Collaboration), Phys. Rev. D **45**, 001448 (1992).
[20] A. Bhatti *et al.*, Nucl. Instrum. Methods A **566**, 375 (2006).
[21] J. Beringer *et al.* (Particle Data Group), Phys. Rev. D **86**, 010001 (2012), and 2013 partial update for the 2014 edition.
[22] T. Sjostrand, S. Mrenna, and P. Skands, J. High Energy

Phys. 05 (2006) 026.
[23] R. Brun, R. Hagelberg, M. Hansroul, and J. Lassalle, CERN-DD-78-2-REV and CERN-DD-78-2.
[24] H. L. Lai, J. Huston, S. Kuhlmann, J. Morfin, F. Olness, J. F. Owens, J. Pumplin, and W. K. Tung (CTEQ Collaboration), Eur. Phys. J. C **12**, 375 (2000).
[25] M. Bauce, FERMILAB-THESIS-2013-27, (2013).
[26] The lepton-like objects used in the misidentification rate measurement are defined starting from the criteria applied for lepton identification in Section III, relaxing the requirements on the lepton isolation in the calorimeters and the fraction of hadronic and electromagnetic energy.
[27] D. Acosta *et al.*, Nucl. Instrum. Methods A **494**, 57 (2002).
[28] *Statistics*, in K. Nakamura *et al.* (Particle Data Group), J. Phys. G **37**, 075021 (2010).
[29] S. Frixione and B. R. Webber, J. High Energy Phys. 06 (2002) 029.
[30] U. Baur and E. L. Berger, Phys. Rev. D **47**, 4889 (1993).
[31] U. Langenfeld, S. Moch, and P. Uwer, Phys. Rev. D **80**, 054009 (2009).
[32] M. Feindt and U. Kerzel, Nucl. Instr. Methods A **559**, 190 (2006).
[33] S. Kretzer, H. L. Lai, F. I. Olness, and W. K. Tung, Phys. Rev. D **69**, 114005 (2004).
[34] U. Baur, T. Han, and J. Ohnemus, Phys. Rev. D **57**, 2823 (1998).
[35] N. Kidonakis and R. Vogt, Phys. Rev. D **68**, 114014 (2003).
[36] M. Cacciari, S. Frixione, M. L. Mangano, P. Nason, and G. Ridolfi, J. High Energy Phys. 04 (2004) 068.